ENVIRONMENTAL ENGINEERING SCIENCE
Volume 37, Number 1, 2019

DOI: 10.1089/ees.2019.0220

Arsenic Adsorption on Iron-Modified Montmorillonite: Kinetic Equilibrium and Surface Complexes

Analia Iriel,[1,2] Jose L. Marco-Brown,[3,*] Maja Diljkan,[2] María Alcira Trinelli,[4,5] María dos Santos Afonso,[6,7] and Alicia Fernández Cirelli[1,2]

[1]*Animal Production Research Institute (INPA/UBA-CONICET), Faculty of Veterinary Science, University of Buenos Aires, Argentina.*
[2]*Institute for Transdisciplinary Water Research (CETA/UBA), Faculty of Veterinary Science, University of Buenos Aires, Argentina.*
[3]*Institute of Environmental Research and Engineering (IIIA), CONICET, UNSAM, University of San Martín, Buenos Aires, Argentina.*
[4]*Institute of Basic, Applied and Environmental Geosciences of Buenos Aires (IGEBA/UBA-CONICET), Buenos Aires, Argentina.*
[5]*Geological Science Department, Faculty of Exact and Natural Sciences (FCEN), University of Buenos Aires (UBA), Buenos Aires, Argentina.*
[6]*Department of Inorganic, Analytical and Physical Chemistry (DQIAQF), Faculty of Exact and Natural Sciences (FCEN), University of Buenos Aires (UBA), Buenos Aires, Argentina.*
[7]*Institute of Chemical Physics of Materials, Environment and Energy (INQUIMAE/CONICET-UBA), University of Buenos Aires, Buenos Aires, Argentina.*

Received: May 20, 2019 *Accepted in revised form: September 5, 2019*

Abstract

As(V) adsorption mechanisms on an iron-modified montmorillonite (Fe-Mt) were studied by analysis from kinetic and equilibrium perspectives, and applicability of Fe-Mt for As(V) removal from groundwater was evaluated. Iron-modified montmorillonite was characterized by Small Angle X-Ray Scattering (SAXS), Wide Angle X-Ray Scattering (WAXS) and scanning electron microscopy technique and an excellent performance for As(V) removal, even at neutral and basic pH values and high conductivity conditions, was determined. Moreover, As(V) adsorption was higher with the increasing of ionic strength of the solution. Both Langmuir and Freundlich models provided a suitable fit to the experimental data, and the maxima adsorption capacity was 6.3 g/kg. Kinetic studies indicated that about 99% of As(V) was removed in the first 30 min of time from a starting concentration of 3 mg/L following a pseudo-second order kinetic. Formation of inner-sphere complexes of As(V) at the surface of Fe-Mt was stated by evaluation of As(V) adsorption in the presence of Cl^-, NO_3^-, and PO_4^{3-} ions and of the zeta potential versus pH curves.

Keywords: adsorption; arsenic; drinking water; modified clay materials

Introduction

Arsenic removal from drinking water is a very important issue in many regions of Latin America, the United States, India, Bangladesh, China, Japan, and other countries. Nowadays, it is estimated that 226 million people worldwide are exposed to unsafe As concentrations in drinking water (Murcott, 2012). Its occurrence in environmental matrices is associated with natural weathering, volcanic emissions, geochemical reactions, and biological activity. Particularly, in Latin America, most of the environmental problems regarding the presence of As are due to its mobilization under natural conditions (Smedley *et al.*, 2005; Litter *et al.*, 2019). Moreover, mining activities, steel industry, combustion of fossil fuels, and use of arsenical pesticides create additional impacts (Apul *et al.*, 2005; Ancelet *et al.*, 2012; Bundschuh *et al.*, 2012; Iriel *et al.*, 2015a). In ground and surface waters, dissolved As is present in inorganic forms either as oxyanions or as neutral species depending on the pH and oxidative conditions (Smedley and Kinniburgh, 2002; Smedley *et al.*, 2005).

More than 100 years ago, it was stated that long-term exposure to drinking water with As, even in lower concentrations, is responsible for several medical disorders that include dermal disorders (Kazi *et al.*, 2009), cancer, and diabetes (Sinha *et al.*, 2007). Several technologies that were able to remove As from aqueous matrices were proposed in the past decades, with the operational volume and the physicochemical properties of raw water together with economic aspects being the most important factors to decide about their applicability (Litter *et al.*, 2012). Conventional large-scale As removal plants mainly use coagulation-flocculation-filtration with polyaluminum chloride or ferric oxide and reverse osmosis-based methods (Litter *et al.*, 2012). Nevertheless, their implementation in small communities is wasteful to

**Corresponding author:* Institute of Environmental Research and Engineering (IIIA), CONICET, UNSAM, University of San Martín, 25 de Mayo Av. and Francia St., San Martín, Buenos Aires, Argentina. *Phone:* +54 911 2162 0334; *E-mail:* josemarcobrown@gmail.com; joseluis.marcobrown@unsam.edu.ar

provide safe water due to the low population density (Bundschuh *et al.*, 2012).

Emerging and innovative technologies that are suitable to isolated rural and periurban areas such as phytoremediation, the use of zerovalent iron, iron/copper bimetallic nanoparticles, iron-based sorbents, photochemical and geological processes, electrochemical technologies, and the use of low-cost materials as adsorbents have ultimately received more attention (Kumar *et al.*, 2008; Litter *et al.*, 2012; Iriel *et al.*, 2015a, 2015b; Babaee *et al.*, 2018; Alvarez-Cruz and Garrido-Hoyos, 2019; Sherlala *et al.*, 2019; Wang *et al.*, 2019; Xu *et al.*, 2019).

Interestingly, constructed wetlands combine several mechanisms implied in As removal such as adsorption, precipitation of metal sulfide, and plant uptake (Chowdhury *et al.*, 2008). In a critical review, the role of microbial activity, organic matter, and redox potential in the fate and transport of As in constructed wetlands was detailed (Chowdhury, 2017). Prototype wetlands planted with *Cyperus haspans* and *Juncus effusus* showed an efficiency close to 90% to remove As from the rejection of the reverse osmosis process (Corroto *et al.*, 2019).

The efficiency of As removal strongly depends on conditions of the proceedings that can be easily adjusted in a treatment plant. Otherwise, in a level home, minimal handling is required. This constitutes the major problem considering that there is a wide range of possibilities in natural waters regarding pH, conductivity, and major ions. Consequently, removal methods that exhibit good results in a lab may be not good enough at field conditions (Bundschuh *et al.*, 2010). The use of geological materials is an economical and sustainable alternative due to the abundance and low cost (Mohan and Pittman, 2007).

Montmorillonite (Mt) has large specific surface area, layered structure, chemical and mechanical stability, and high cation exchange capacity (CEC). It is found in large deposits around the world and has received attention in both academic and industrial research due to its promising and peculiar features such as adsorbent material, low cost, or for reinforcing polymer nanocomposites, among others (Bhattacharyya and Gupta, 2008; Zhu *et al.*, 2016; Bee *et al.*, 2018). Particularly, pillared and modified clay minerals are interesting materials because of their possibility of being tuneable in terms of their properties (Timofeeva *et al.*, 2009). These materials exhibit multi-charged sites, large surface area, high interlayer space, and thermal stability (Gil *et al.*, 2011).

Pillared materials obtained by solutions containing iron or titanium had demonstrated excellent performance in the adsorption of oxoanions of As(III) and As(V) from aqueous solutions (Lenoble *et al.*, 2002; Li *et al.*, 2012). Regarding modified clay minerals, obtaining it is cheaper than the pillared ones since they do not need to be heated during their synthesis.

Several studies were performed on iron-modified clays materials to evaluate their performance for As removal. Grygar *et al.* (2007) focused on the study of synthesis procedures to obtain information about iron species formed in these materials. These authors also evaluated their performance regarding As adsorption, concluding that the sorption capacity increases with the Fe/OH ratio during the synthesis. Luengo *et al.* (2011) studied the adsorption/desorption kinetics of arsenate on Fe-modified montmorillonite at several pH values, stirring rates, and As initial concentrations. Moreover, Ren *et al.* (2014) reported the adsorption parameters of As adsorbed onto Fe-modified montmorillonite.

Besides these previous papers, there are still questions to be addressed to understand better the applicability of these materials to remove As from natural waters. In a recent work, Bhowmick *et al.* (2014) presented the kinetic parameters and mechanisms for the As adsorption onto a montomorillonite-supported nanoscale zero-valent iron where the ion's competence and pH were considered. Although most of the cited articles in this work evaluate the adsorption at several pH, the maxima adsorption capacities are determined at the most favorable pH condition. Moreover, studies considering conductivity of the media are scarce. In this context, we are interested in evaluating the As(V) adsorption onto iron-modified clay minerals from a kinetic and equilibrium perspective at natural groundwater conditions and that are the principal mechanisms involved.

Materials and Methods

Reagents

All the reagents used were of analytical grade and used without further purification. A stock As(V) solution of 1,000 mg/L was prepared by dissolving 4.4570 g of the salt $Na_3AsO_4.7H_2O$ (Biopack) in a volume of 1 L by using milliQ water (Millipore GmbH). Working solutions were prepared by dilution to obtain As(V) concentrations ranging from 0.1 to 12 mg/L, which is the range documented for As concentration in groundwater in Latin America (Bundschuh *et al.*, 2012; Litter *et al.*, 2019). The salt $Fe(NO_3)_3.9H_2O$ (Aldrich) was used for the synthesis of the modified clay material. To adjust pH of the solutions, HNO_3 (Suprapur®; Merck) and KOH solutions (Cicarelli) were utilized. The effects of the counterion and the ionic strength were evaluated with KNO_3 (Merck), NaCl (Cicarelli), and $Na_3PO_4.12H_2O$ (Sigma-Aldrich).

Clay materials

Montmorillonite API number 26, Clay Spur, Wyoming, was provided by Ward's Natural Science Establishment, Inc. Mt was manually milled in an agate mortar and sieved to a particle size lesser than 125 μm. The main properties of raw material, reported in a previous work (Marco-Brown *et al.*, 2014), are: CEC 138 meq 100 g^{-1} determined by the formaldehyde method (Reeve and Sumner, 1971), purity >98% determined by X-ray diffraction (XRD) (Rietveld, 1969), and isoelectric point at pH = 3.2 (diffusion potential method) (Tschapek *et al.*, 1989). The structural chemical formula that includes the isomorphic substitutions ($[(Si_{3.94}A_{l0.06})(Al_{1.56}Fe_{0.18}Mg_{0.26})O_{10}(OH)_2]M^+_{0.32}$) was determined from the chemical analysis following the method of Siguín *et al.* (1994).

Modified clay material (iron modified montmorillonite [Fe-Mt]) was prepared according to Marco-Brown *et al.* (2012). Briefly, a solution of Fe(III) 1 M was prepared by dissolution of the salt at room temperature with vigorous stirring and the slow addition of a solution of KOH (2 M), until reaching a molar ratio of $OH^-/Fe = 2$. The solution was kept at room temperature for 4 h for aging. Mt was added to the Fe(III) solution to obtain an Fe/Mt ratio of 60 mmol Fe g^{-1} Mt. The mixture was allowed to react, stirring at room temperature for 12 h. The solid was separated by centrifugation

and washed with deionized water until a conductivity value lower than 10 μS was reached.

Surface characterization of clay materials

Nitrogen adsorption–desorption isotherms were recorded at 77 K by using a Micromeritics ASAP 2010 instrument. All samples were degassed at 150°C before measurement. The specific surface area was calculated by using the BET method (Brunauer *et al.*, 1938).

Mt and Fe-Mt samples were characterized by Small Angle X-Ray Scattering (SAXS) and Wide Angle X-Ray Scattering (WAXS) to determine changes in the interlayer spacing. Data were obtained at the D01A SAXS line workstation of the Brazilian Synchrotron Light Source (LNLS), Campinas, Brazil, by using a wavelength of 0.155 nm and a sample to detector distance of 491.334 mm. The recorded scattering vector (q) ranged from 0.25 to 5.9 nm. Measurements were made at room temperature and registered in a 2D-CCD detector (MAR-USA 165 mm).

The morphology and surface chemical analysis of Mt and Fe-Mt were determined by scanning electron microscopy (SEM) using an FEG-SEM Zeiss Supra 55vp coupled with an energy-dispersive X-ray analyzer (EDX) that provides a qualitative and semiquantitative composition of the sample surface.

The zeta potential was achieved through the measurement of electrophoretic mobility values that were converted by using the Smoluchowski equation. Fe-Mt samples with or without As(V) adsorbed were dispersed in solutions of 1, 10, and 25 mM KNO_3. The pH was adjusted by adding drops of KOH or HNO_3 from 2 to 11. Measurements were performed by using a dosage of 200 mg/L with Zeta Plus light-scattering zeta potential analyzer (Brookhaven Instruments Co.).

Adsorption batch experiments

Batch experiments were conducted to determine the kinetic and equilibrium parameters of the As(V) adsorption onto clay material particles. To evaluate the extension of the As adsorption regarding the solution properties, experiments were conducted at pH 4, 6, and 8; whereas the influence of the ionic strength was determined by using solutions adjusted at 1, 10, and 25 mM KNO_3 (that corresponds to conductivities of 160, 1,300, and 3,300 μS, Hanna, HI 255). Experiments were also performed in the presence of NaCl and Na_3PO_4 electrolytes. For that, 0.25 mg of adsorbent (Mt or Fe-Mt) was dispersed in 1×10^{-2} mM As(V) solutions with a molar ratio of 1:100 arsenic:electrolyte.

Kinetic studies were performed to evaluate the effect of the contact time on the As(V) adsorption. Thus, 300 mL of As(V) solution of 1 mg/L with 0.15 g of adsorbent (Fe-Mt) at constant pH = 8 and ionic strength of 1 mM KNO_3 was mechanically stirred (300 rpm) for 24 h. During this time, several aliquots were taken and the supernatant was separated by centrifugation and filtration (cellulose nitrate membrane, 0.45 μm). Samples were acidified to 0.5% with HNO_3 and stored at 4°C until the As measurement.

Equilibrium experiments were performed with As(V) working solutions with concentrations ranging from 0.1 to 12 mg/L and a dose of 0.5 g/L of adsorbent (Fe-Mt), at constant pH = 8. Dispersions were maintained on agitation at room temperature for 6 h and then As concentration was evaluated in the supernatant.

Arsenic measurements

As(V) concentration in sampled solutions was measured by Inductively coupled plasma-optical emission spectrometry (ICP-OES, Optima DV 2000; Perkin Elmer) according to the methodology reported by Iriel *et al.* (2015a). From these measurements, the clay mineral adsorption coverage Γ_e for As(V) was calculated as:

$$\Gamma_e = \frac{(C_0 - C_e)V}{m} \quad (1)$$

where both C_0 and Ce are As(V) concentration at initial and equilibrium time in the solution (mg/L), respectively; m is the clay mineral mass (g); and V is the volume of the solution (L). In adsorption kinetic experiments, Γ_t is calculated in a similar way to Γ_e but C_e is replaced by C_t (As(V) concentration at a given time *t*). As(V) removal (%) was estimated as:

$$\%\ \text{Removal} = \frac{(C_0 - C_e)\text{x } 100}{C_0} \quad (2)$$

Kinetic and equilibrium adsorption models

Kinetic analysis. Kinetic parameters from adsorption process have been obtained by fitting experimental data to pseudo-first order (PFO), pseudo-second order (PSO), and intra-particle diffusion model (IDM) equations (Areco *et al.*, 2013; Haerifar and Azizian, 2013; Marco-Brown *et al.*, 2014) and to the mixed surface reaction and diffusion-controlled adsorption kinetic model (MSR/DCK), recently proposed (Haerifar and Azizian, 2013). For further information about kinetic models used in this work, see Supplementary Data.

Equilibrium studies. Adsorption isotherms are extremely helpful for optimizing the use of adsorbent materials, because they describe the nature of the interaction between the sorbate and the adsorbent. The analysis of the experimental data is useful for the practical design and operation of adsorption systems. There are several expressions used for description of adsorption isotherms, with Langmuir and Freundlich models being the most widely applied for the interpretation of adsorption processes in a wide variety of adsorbents. For further information regarding isotherm models used in this work, see Supplementary Data.

Statistical analysis

Analysis was performed by Sigmaplot 11.0 software to determine adsorption isotherm and kinetic parameters of the cited models. Infostat® statistical software (Di Rienzo *et al.*, 2011) was used to perform the analysis of variance and the Pearson correlations. Previously, a normal distribution for the whole data set was confirmed by using the Shapiro-Wilks modified test and variance homogeneity was proved with the Levene test.

Results and Discussion

Characterization of clay materials

All materials presented a type II nitrogen adsorption–desorption isotherm (Fig. 1A) with a type H3 hysteresis

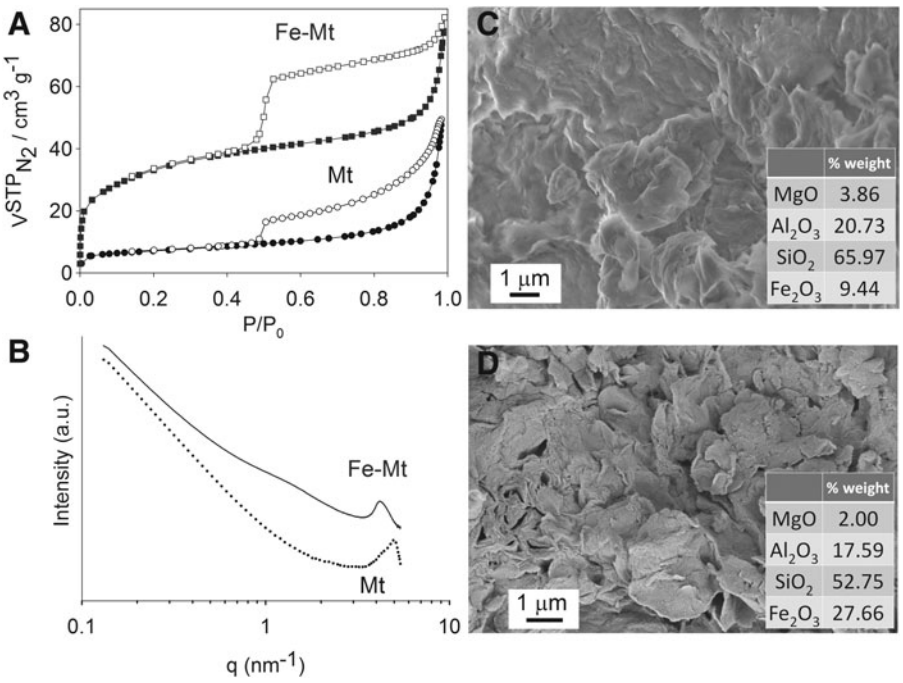

FIG. 1. **(A)** N_2 adsorption/desorption isotherms on Mt and Fe-Mt. **(B)** SAXS/WAXS patterns for Mt and Fe-Mt. **(C, D)** SEM images of Mt and Fe-Mt, respectively. *Insets* in **(C, D)** oxide (%) determined by EDX in Mt and Fe-Mt, respectively. EDX, energy-dispersive X-ray analyzer; Fe-Mt, iron-modified montmorillonite; Mt, montmorillonite; SAXS, small angle X-ray scattering; SEM, scanning electron microscopy; WAXS, wide angle X-ray scattering.

associated with low porosity materials formed by sheet agglomerations. The specific surface areas were 24 and 107 m^2/g and the pore volumes were 0.04 and 0.09 cm^3/g for Mt and Fe-Mt, respectively. WAXS and SAXS patterns for Mt and Fe-Mt samples are shown in Fig. 1B, where an increment from 1.26 to 1.49 nm in the basal space was detected, suggesting the intercalation of Fe oligomers into the interlayer space. The SEM image of Mt (Fig. 1C) showed face-to-edge contact between the particles with random orientation, and no formation of domains (group of particles that act as a unit) or clusters (group of domains that act as a unit), whereas agglomerates were identified. The SEM image of Fe-Mt is shown in Fig. 1D, where pore spaces can be identified; particles with sizes between 100 and 500 nm corresponding to coaggregate or iron oxide particles on the surface and randomly dispersed are observed. Insets in Fig. 1C and D show the clay mineral composition expressed as oxides (%), where the Fe incorporation on Fe-Mt was evidenced by the increase of Fe_2O_3 (%) from 9.44 to 27.66.

Influence of pH and of coexisting ions

The dependence of the solution pH on the solute adsorption is mainly related to the surface functional groups of the sorbent and the charge of the species into the solution. Figure 2A showed the adsorption capacities for Mt and Fe-Mt in contact with an As(V) solution of 3 mg/L equilibrated at pH 4, 6, and 8. Results indicated that Fe-Mt had a maxima value of 5.3 g As kg^{-1} at pH 4, which corresponds to 90% of the initial concentration. However, a significant diminution at pH 6 was observed where the adsorption (%) was nearly 80%; whereas at pH 8, a minimal adsorption of 2.9 g As kg^{-1} that corresponds to the 50% was observed. From H_3AsO_4 acidity, constant values (pKa_1: 2.28; pKa_2: 6.97 and pKa_3: 11.6) (Wang *et al.*, 2017) can be estimated, proving that the predominant species are $H_2AsO_4^-$ at pH = 4, $H_2AsO_4^-$ and $HAsO_4^{2-}$ at pH = 6, and $HAsO_4^{2-}$ at pH = 8. Taking into account this feature where the As(V) removal (%) diminishes as the pH increases, it can stated that Fe-Mt exhibited an anionic adsorption profile.

Similar results have been reported for the adsorption of picloram (anionic herbicide) on raw clays and Fe oxides modified motmorillonite (Marco-Brown *et al.*, 2012, 2014,

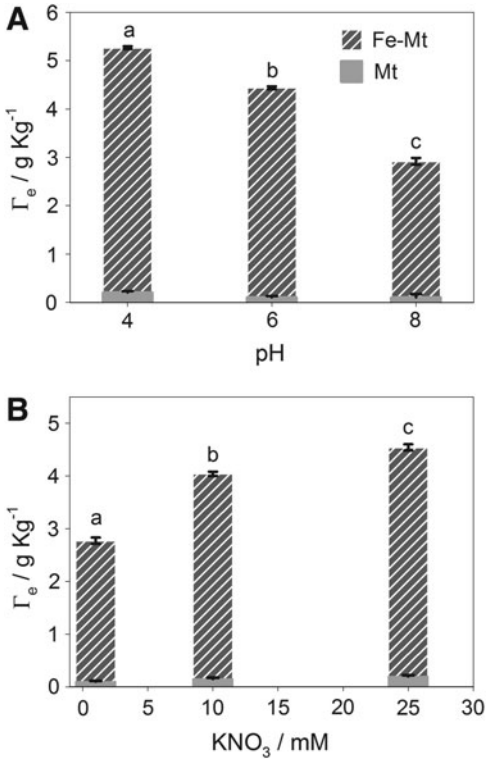

FIG. 2. Adsorption of As(V) from a 3 mg/L starting solution by Mt and Fe-Mt (clay mineral dosage of 5 mg/L) **(A)** as a function of pH under ionic strength of KNO_3 1 mM; and **(B)** as a function of ionic strength at pH 8. Error bars are standard errors, and *different letters* represent significant differences at $p < 0.05$.

2015, 2019) and nitrate adsorption on biochars (Chintala *et al.*, 2013). Antelo *et al.* (2005) reported the adsorption of arsenate on goethite varies with the ionic strength (0.1–0.01 M KNO_3) and pH (4–10). They also observed that the As adsorption decreases as the pH increases. Analogous results have been reported for the adsorption of As(III) and As(V) onto variable charge soils (Xu *et al.*, 2010). Regarding our results, it was observed that even when Fe-Mt had a better performance in acidic media, in both neutral and basic conditions, Fe-Mt possess an excellent efficiency for As(V) removal. For instance, nearly 80% and 50% of arsenate was removed at pH 6 and 8, respectively. This is a very important result that indicates that modified Fe-Mt is able to be used in natural waters without the previous acidification procedure, and, consequently, it could be implemented at a household level.

The effect of ionic strength on the As(V) adsorption process was evaluated to determine the capability of these materials to remove As(V) anions in natural waters with different salt content. Moreover, the presence of electrolytes in the media allows discerning between the specific and nonspecific nature of the binding evaluating the changes in As(V) adsorption (Partey *et al.*, 2009). In particular, changing the background electrolyte concentration influences adsorption in at least two ways: (1) by affecting the interfacial potentials and (2) by the competition between the electrolyte anions and the anionic adsorbing species for the available sites for adsorption (Hayes *et al.*, 1988).

Figure 2B shows a significant enhancement of As(V) adsorption as the KNO_3 concentration increases, as has been indicated for anion adsorption on hydrous oxide materials (Hayes *et al.*, 1988; Liu *et al.*, 2008). A marked reduction of anion adsorption with increasing ionic strength suggests an outer-sphere complex formation. Otherwise, when anion adsorption is relatively unaffected by changes in ionic strength, the adsorption process could be associated with an inner-sphere complex formation. Results presented in Fig. 2B are not only indicative of an inner-sphere adsorption mechanism for arsenate onto Fe-Mt but also indicate that the use of Fe-Mt as As(V) adsorbent is appropriate in natural waters with high conductivity. The competition of As(V) adsorption (at pH 8) with other ions such as chloride (Cl^-) and phosphate (PO_4^{3-}) was determined in Fe-Mt samples in this study, and the results indicated that As(V) removal by Fe-Mt increased in the following order: PO_4^{3-} (0.96%) < Cl^- (30.64%) < NO_3^-(47.15%), showing a greater decrease in arsenic adsorption in the presence of phosphate. Adsorption from strong anions such as Cl^-, NO_3^-, Br^-, and ClO_4^- to functional groups on the surface of mineral acids occurs through outer-sphere complexation processes that are driven mainly by electrostatic forces (Essington, 2004; Marco-Brown *et al.*, 2017b). The adsorption of phosphate on metal oxides has been reported to occur by inner-sphere complexation processes, interacting with a metal center via formation of monodentate or bidentate complexes or with two adjacent metal centers by forming a bridge complex (Higuchi and Connors, 1965; He *et al.*, 1997; Marco-Brown *et al.*, 2017b). Therefore, these results could indicate that As(V) adsorption onto the surface of Fe-Mt occurs by forming an inner-sphere complex. To confirm the inner-sphere complex formation, the zeta potential of Fe-Mt particle dispersions with and without adsorbed As(V) was determined at different pH values. Results are shown in Fig. 3.

Zeta potential for Fe-Mt dispersions in KNO_3 solutions showed negative values in the entire range of studied pH (Fig. 3A). The distribution observed for Fe-Mt was a combination between the zeta potential observed for Mt (Marco-Brown *et al.*, 2012) and for iron(III) (hydr)oxides (Tombácz *et al.*, 2001). The iron incorporation in the clay mineral

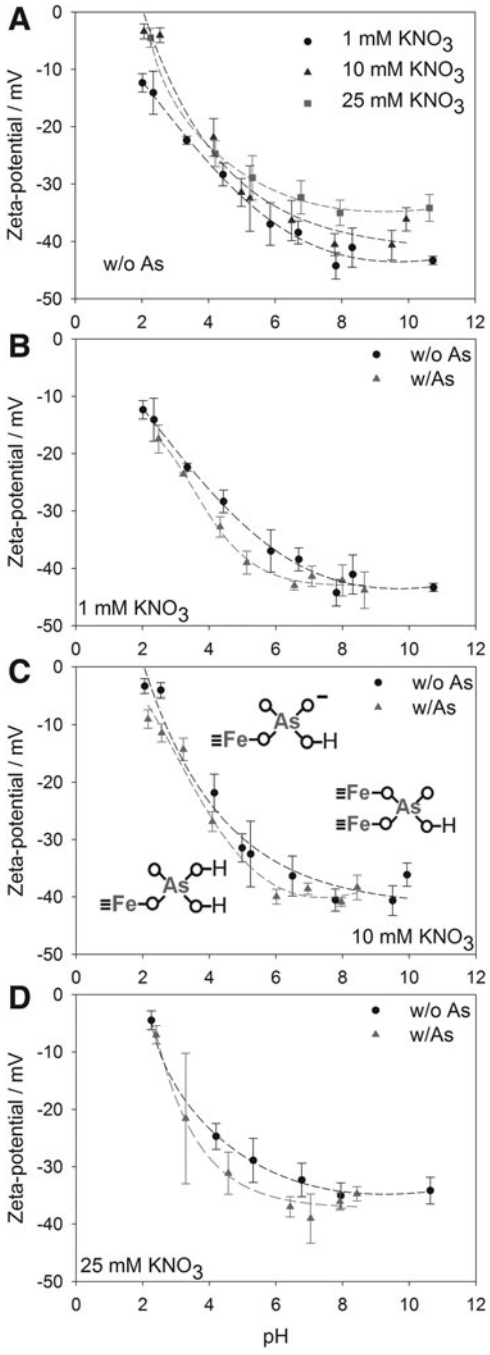

FIG. 3. Zeta potential of Fe-Mt particles as a function of pH. **(A)** Fe-Mt dispersed in 1, 10, and 25 mM of KNO_3; **(B–D)** Fe-Mt with (w/As) and without (w/o As) As(V) adsorbed and dispersed in 1, 10, and 25 mM of KNO_3, respectively. The *dashed lines* are placed on graphs as a guide to the eye. *Insets* in **(C)** are the main As(V) surface complex species in a different pH domain.

structure changed the surface properties by adding iron metallic centers. In addition, Fe(III) has a different acid–base behavior than the groups normally present on the Mt surface (sylanol and aluminol). The variation of zeta potential values with ionic strength observed in Fig. 3A is typical of hydrous ferric oxide materials (Stumm, 1992). From Fig. 3A, a point zero charge (PZC) of Fe-Mt could be estimated around pH 2.

The iron atoms located at the Fe-Mt surface are coordinated to oxygen atoms, where they can be in several forms such as protonated ($\equiv FeOH_2^+$), neutral ($\equiv FeOH$), or deprotonated ($\equiv FeO^-$) depending on the solution pH. At pH values lower than 4, the reaction may occur at Fe-Mt surface as is indicated in Equation (3), where the interaction of the main As(V) species at pH 4 ($H_2AsO_4^-$) with surface sites occurs by forming a monodentate inner-sphere complex ($\equiv FeOAsO_3H_2$) and the leaving group is the hydroxyl anion. Similar reactions can be described for $\equiv FeOH_2^+$ and $\equiv FeO^-$ surface sites and with water and/or hydroxyl anion being the leaving groups. The monodentate complex is formed without changes in the surface charge or with an increase in the negative charge depending on the surface charge balance. Then, the surface charges of Fe-Mt with As(V) and without As(V) adsorbed had a similar result, as is observed in Fig. 3B–D. This effect was observed at the three KNO_3 concentrations: 1, 10, and 25 mM.

$$\equiv FeOH + H_2AsO_4^- \quad \Leftrightarrow \quad \equiv FeOAsO_3H_2 + OH^- \quad (3)$$

At a pH around 6, the reactions that may occur at the Fe-Mt surface are indicated in Equations (3) and (4). The interaction of main As(V) species at pH 6 ($H_2AsO_4^-$ and $HAsO_4^{2-}$) with surface sites occurs by forming a new monodentate inner-sphere complex ($\equiv FeOAsO_3H^-$), and the leaving groups are hydroxyls in both cases. Nevertheless, the surface charge of Fe-Mt with As(V) adsorbed is much more negative than Fe-Mt without As(V) adsorbed (Fig. 3B–D). The main reaction on the Fe-Mt surface is represented in Equation (4).

$$\equiv FeOH + HAsO_4^{2-} \quad \Leftrightarrow \quad \equiv FeOAsO_3H^- + OH^- \quad (4)$$

The monodentate surface complex $\equiv FeOAsO_3H_2$ may suffer acid–base dissociation and be converted to the second monodentate surface complex, $\equiv FeOAsO_3H^-$, by loss of an acidic proton, increasing the negative charge on the surface, as is indicated in Equation (5). Similar results had been informed for the adsorption of inorganic and organic anionic molecules on hydrous ferric oxides, raw and modified Mt materials (dos Santos Afonso and Stumm, 1992; Khoury *et al.*, 2010; Marco-Brown *et al.*, 2015; Flores *et al.*, 2018).

$$\equiv FeOAsO_3H_2 \quad \Leftrightarrow \quad \equiv FeOAsO_3H^- + H^+ \quad (5)$$

As the pH increases, the charge difference between Fe-Mt with and without As(V) adsorbed samples is becoming smaller and the slope of the zeta potential versus pH for Fe-Mt with the As(V) adsorbed sample becomes flat. At a pH around 8, the reactions that may occur at the Fe-Mt surface are indicated in Equations (4) and (6). The interaction of the main As(V) species at pH 8 ($HAsO_4^{2-}$) with surface sites may occur by forming a monodentate [Eq. (4)] and/or bidentate [Eq. (6)] inner-sphere complexes, and the leaving groups are hydroxyls in both cases. Nevertheless, the surface charge of Fe-Mt with As(V) adsorbed is similar compared with Fe-Mt without As(V) adsorbed (Fig. 3B–D), demonstrating that the main reaction occurred at the Fe-Mt surface at pH 8, as indicated in Equation (6).

$$2 \equiv FeOH + HAsO_4^{2-} \quad \Leftrightarrow \quad (\equiv FeO)_2AsO_2H + 2OH^- \quad (6)$$

In Fig. 3C (insets), the main As(V) surface complexes species at different pH domains were schematized. These results provide indirect and conclusive evidence about the formation of surface complexes between the surface of the Fe-Mt particles and As(V), confirming an inner-sphere complex formation.

Adsorption kinetics

Due to the low quantity of As(V) adsorbed onto Mt (lower than 5%), kinetics and adsorption parameters were determined by using only Fe-Mt as adsorbent. Kinetic experiments were performed while evaluating the As(V) concentration from the solution as a function of time. Surface coverage of As(V) on Fe-Mt was calculated by using Equation (1) and plotted according to PFO, PSO, IDM, and MSR/DCK models (Supplementary Data), as is shown in Fig. 4. The first fitting indicated that the Lagergren model did not fit the experimental data due to R^2 being lower than 0.01 (Fig. 4A). Regarding the PSO model, an excellent agreement was observed over the entire range of time (Fig. 4B). In addition, the plot of q_t versus $t^{1/2}$ for As(V) adsorption on Fe-Mt is shown in Fig. 4C. The diffusion kinetic plots exhibited the three-stage linearity, which indicates that two or more steps occur in the adsorption processes (Peng *et al.*, 2016; Marco-Brown *et al.*, 2017a, 2018). The first portion (corresponding to initial times) had been related to high adsorption rate on the external surface of the adsorbent, which has enough available adsorption sites. Afterward, the adsorption rate diminishes due to the difficulty in As(V) reaching the adsorption sites in the inner pores of Fe-Mt, where the intra-particle diffusion is the rate-controlling step. The k_{id} and C constant values were obtained from the slope and intercept from the linear regression of the second portion (intermediate times) of the curve, respectively (Doğan *et al.*, 2009). In addition, the curve did not pass through the origin, which indicates that diffusion through the pores is not the limiting factor (Guo *et al.*, 2014). The C value [Eq. (S3), Supplementary Data] reflects the boundary layer effect. The larger the intercept of the plot, the greater the contribution of the surface sorption in the rate-limiting step. Finally, the third portion is the final equilibrium stage, where the intra-particle diffusion starts to slow down due to the low As(V) concentration in solution (Sun and Yang, 2003). Hence, the three-stage linearity of intra-particle diffusion plots confirmed the presence of both surface adsorption and intra-particle diffusion (Guo *et al.*, 2014) as was proposed by PSO modeling. Thus, the adsorption process has a complicated nature involving both surface adsorption and intra-particle diffusion (Doğan *et al.*, 2009). In conclusion, the adsorption of As(V) on Fe-Mt involved a two-step mechanism, a rapid one occurring on the external surface followed by a slower process that occurs on the pores by interlayer diffusion as was previously reported (Luengo *et al.*, 2011).

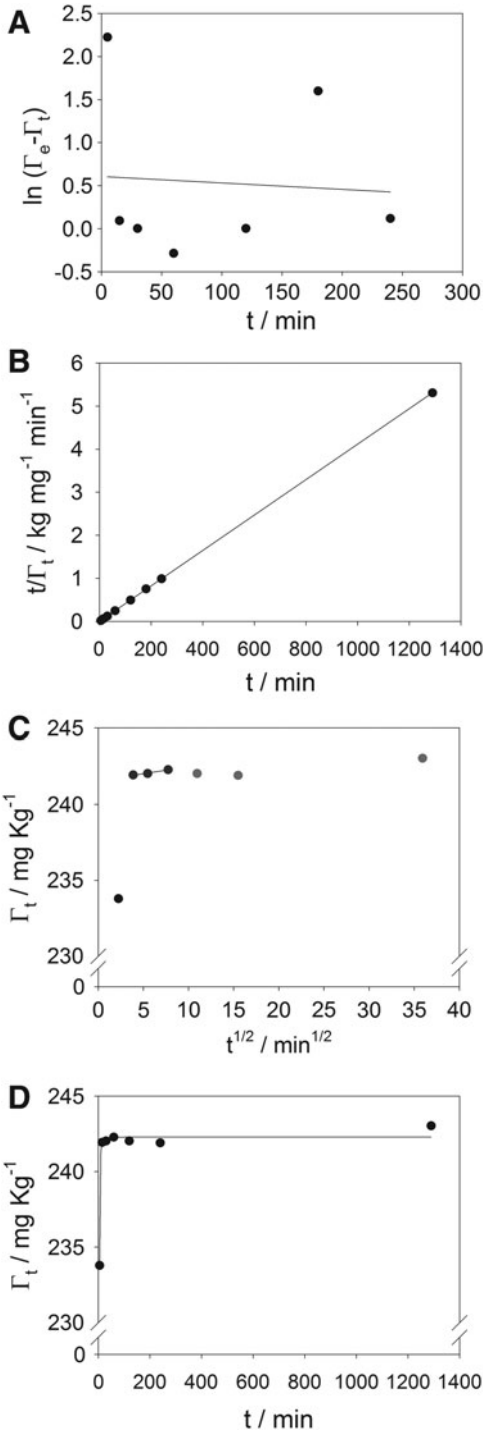

FIG. 4. Fitting of experimental data of As(V) adsorption onto Fe-Mt at As(V) initial concentration 3 mg/L, solid dosage 0.5 g/L, pH 8, and ionic strength 1 mM KNO_3. **(A)** Pseudo-first order, **(B)** pseudo-second order, **(C)** intra-particle diffusion, and **(D)** mixed surface reaction and diffusion-controlled kinetic models.

Haerifar and Azizian (2013) have proposed a new model that can be used when diffusion and surface reaction control the overall rate of the process at the solid/solution interface. In these cases, the mixed surface reaction and diffusion-controlled kinetic model can be applied, where the surface coverage as a function of time is modeled according to Equation (S4) (Supplementary Data) (Fig. 4D). The obtained value of τ is >0, which means the presence of diffusion in conjunction with surface reaction. A μ_{eq} value near to 1 indicated that As(V) was completely removed from the solution by Fe-Mt. Further, the good correlation of the MSR/DCK model with the experimental data is indicated by the high value of R^2 and the Γ_e value of 242.28 mg/kg. Also, the τ value confirms the previous results obtained by IDM adjustment, indicating that As(V) adsorption on Fe-Mt occurs through both surface adsorption and intra-particle diffusion processes. Kinetic parameters derived from the evaluated models are presented in Table 1.

Table 1. Parameters Obtained for Kinetic Models for As(V) Adsorption onto Fe-Mt

Model	*Parameter*	*Value*
PFO	$k_1 \times 10^4$ (min^{-1})	7.47
	R^2	<0.005
PSO	$k_2 \times 10^3$ (kg/[mg·min])	5.01
	Γ_e (mg/kg)	243.11
	R^2	0.9999
IDM	k_{id} ($mg \cdot kg^{-1} \cdot min^{-1/2}$)	0.091
	C (mg/kg)	241.57
	R^2	0.9756
MSR/DCK	Γ_e (mg/kg)	242.28
	μ_e	0.999
	k (L/[mg·min])	67.31
	τ (min)	1.05
	R^2	0.9870

Fe-Mt, iron-modified montmorillonite; IDM, intra-particle diffusion model; MSR/DCK, mixed surface reaction and diffusion-controlled kinetic model; PFO, pseudo-first order; PSO, pseudo-second order.

Adsorption isotherm models

Equilibrium studies were performed to determine the adsorption mechanism of As(V) on Fe-Mt and the adsorption maxima capacity of the synthesized material. For that, batch Fe-Mt dispersions with As(V) concentrations ranging from

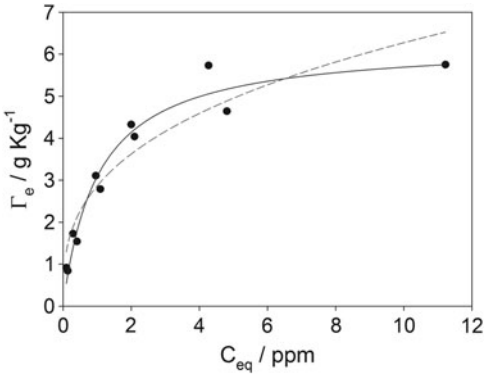

FIG. 5. As(V) adsorption isotherms on iron-modified clay material at Fe-Mt dosage 0.5 g/L, pH 8, and ionic strength 1 mM KNO_3. *Solid* and *dashed lines* were obtained by using Langmuir and Freundlich models, respectively.

Table 2. Langmuir and Freundlich Parameters for As(V) Adsorption on Fe-Mt at Solid Dosage 0.5 g/L, pH 8, and Ionic Strength 1 mM KNO_3

Model	*Parameter*	*Value*
Langmuir	Γ_{max} (g/kg)	6.28
	K_L (L/mg)	0.966
	R^2	0.9597
Freundlich	K_F	2.86
	$1/n$	0.341
	R^2	0.8988

0.1 to 12 mg/L were equilibrated at pH 8 and the ionic strength was set at 1 mM KNO_3. The ratio between the quantity of As(V) adsorbed onto the Fe-Mt particles and the remaining into the solution was fitted to the Freundlich and Langmuir models (Supplementary Data).

From Fig. 5, it is observed that either the Langmuir or Freundlich equations [Eqs. (S5) and (S6), Supplementary Data] are applicable to adsorption experimental data. In the first model, the affinity between sorbent and sorbate is represented by the constant K_L. In general, for good sorbents high Γ_{max} and high K_L are desirable. The K_L for As(V) sorption on Fe-Mt expressed as L/mg was 0.966 (Table 2). The same behavior was observed for the adsorption of As(V) onto zero-valent ions on Mt, where a K_L value of 0.005 L/mg was reported (Bhowmick *et al.*, 2014). Moreover, the Γ_{max} for As(V) obtained from the Langmuir model (6.28 g/kg) is near to the experimental one. In addition, both are within the range reported earlier for As(V) adsorption on iron clay material: 4 g/kg (Lenoble *et al.*, 2002) and 7.6 g/kg (Luengo *et al.*, 2011) at more acidic pH values.

The Fe-Mt performance to remove As(V) was compared with that of other clay minerals in Table 3.

From Table 3, it should be noticed that the synthetic routes of mineral materials affect the performance with regard to As removal. This is a very important issue to be considered due to the cost of the modified material being associated with the synthesis procedures. In addition, it is observed that the final Fe content needs to be optimized. Regarding their implementation at a domiciliary level, it is necessary to provide data according to the natural conditions of pH and conductivity to assure their applicability to achieve safe As concentration for drinking water.

The study of low-cost adsorbents for As(V) removal has a promising future in the development of technologies aimed at mitigating the problem of As in drinking water in periurban

Table 3. Comparison of Adsorption Capacities Reported in the Literature for As(V) on Modified Clays

Sorbent	*Experimental conditions*	Γ_{max}, *g/kg*	*Applied adsorption isotherms and kinetic models*	*References*
Nanoscale zero-valent iron on montmorillonite	pH 7, contact time: 4 h, sorbent dosage: 1.26 g/L.	45.5	Langmuir and Freundlich isotherms, PSO kinetics. Adsorption diminishes at basic pH values. PO_4^{3-} competence decreased the As(V) adsorption.	Bhowmick *et al.* (2014)
Fe-Mt	Without pH adjustment, contact time 20 min, sorbent dosage 4 g/L.	8.85	Langmuir adsorption isotherm, PSO kinetics.	Ren *et al.* (2014)
CTMAB-Fe-Mt	Without pH adjustment, contact time 20 min, sorbent dosage 4 g/L.	15.15	Langmuir adsorption isotherm, PSO kinetics.	Ren *et al.* (2014)
Fe-Mt	pH 6, contact time 24 h, sorbent dosage noninformed.	22	Adsorption isotherm models and kinetic analysis were not considered. As sorption is enhanced with increasing amounts of Fe in the modified mineral.	Grygar *et al.* (2007)
Goethite	Without pH adjustment; contact time 4 h, sorbent dosage 1.6 g/L.	4	Adsorption isotherm models and kinetic analysis were not considered.	Lenoble *et al.* (2002)
Amorphous iron hydroxide	Without pH adjustment; contact time 4 h, sorbent dosage 1.6 g/L	7	Adsorption isotherm models and kinetic analysis were not considered.	Lenoble *et al.* (2002)
Pillared Fe-Mt	Without pH adjustment; contact time 4 h, sorbent dosage 1.6 g/L.	4	Adsorption isotherm models and kinetic analysis were not considered.	Lenoble *et al.* (2002)
Fe-Mt	pH 4.5–9; sorbent dosage 0.26 g/L.	3.9 at pH = 6; 1.5 at pH = 9	Adsorption/desorption kinetics studies. Models were not applied to data analysis.	Luengo *et al.* (2011)
Fe-Mt	pH: 8, contact time 20 min, sorbent dosage: 0.5 g/L.	6.28	Langmuir and Freundlich isotherm models, PSO kinetics mechanism, inner-sphere complexes of As(V) at surface sites.	This work

or isolated rural areas lacking centralized water supplies. Adsorption-based methods of treatment could be applied along or in combination with oxidation–adsorption–coagulation/flocculation methods. These types of technologies are affordable for low economic income and resource populations due to their ability to work with small-scale equipment and treat small volumes of water to supply small communities or individual houses. Their designs are simple, and their installation and maintenance can be easily handled by the local population (Litter *et al.*, 2012). Nevertheless, the use of these technologies at low or medium scale could have the disadvantage of an inadequate handling and disposal of the generated wastes. In this sense, it is important to have efficient communication during the transference of the technology.

Conclusions

Montmorillonite was modified in this work with the intercalation of iron oligomers, and it is proposed as an adsorbent material for As(V) removal from groundwater in small-scale processes. Fe-Mt was synthesized through a low-cost method, and its As(V) adsorption capacity was evaluated by varying parameters such as pH or ionic strength.

The iron modification process of montmorillonite led to a basal space expansion as well as a BET surface value and microporosity increment of the material with respect to raw montmorillonite. Moreover, a modification of active surface sites occurred with the deposition of iron oxides. Structure and surface site modification led to Fe-Mt possessing an extraordinary removal power of As(V) from contaminated water with respect to raw montmorillonite and other adsorbents.

The arsenic adsorption capacity of Fe-Mt had a strong dependence on the physicochemical properties of solutions. Particularly, adsorption capacity was higher at low pH values; nevertheless, good performance was observed at neutral pH values. Regarding ionic strength, adsorption capacity increases with KNO_3 concentration. This result suggested that Fe-Mt could be appropriate for use in As(V) removal processes without previous treatment.

Equilibrium adsorption data were successfully fitted to the Langmuir and Freundlich models. A maximum adsorption capacity of 6.3 g/kg and a K_L value of 0.966 L/mg were determined by fitting experimental data to the Langmuir model. The time of contact necessary to reach the equilibrium condition was around 20 min. Also, it was determined that the adsorption process followed a PSO law. In addition, the suitable fitting to the IDM and MSR/DCK models indicated that not only a surface reaction controls the rate of the process but a diffusion reaction is also important.

Finally, it was stated that As(V) reacts with iron surface sites on Fe-Mt through the formation of inner-sphere complexes.

Author Disclosure Statement

A.I., J.L.M-B., M.A.T, and A.F.C. are members of Consejo Nacional de Investigaciones Científicas y Técnicas (CONICET). All other authors have no competing financial interests.

Funding Information

The authors gratefully acknowledge the Consejo Nacional de Investigaciones Científicas y Técnicas (CONICET) and the Agencia Nacional de Promoción Científica y Tecnológica (ANPCYT) for the financial support (PICT 2015-1260 and PICT 2015-2010).

Supplementary Material

Supplementary Data

References

Alvarez-Cruz, J.L., and Garrido-Hoyos, S.E. (2019). Effect of the mole ratio of Mn/Fe composites on arsenic (V) adsorption. *Sci. Total Environ.* 668, 47.

Ancelet, T., Davy, P.K., Mitchell, T., Trompetter, W.J., Markwitz, A., and Weatherburn, D.C. (2012). Identification of particulate matter sources on an hourly time-scale in a wood burning community. *Environ. Sci. Technol.* 46, 4767.

Antelo, J., Avena, M., Fiol, S., López, R., and Arce, F. (2005). Effects of pH and ionic strength on the adsorption of phosphate and arsenate at the goethite-water interface. *J. Colloid Interf. Sci.* 285, 476.

Apul, D.S., Gardner, K.H., Eighmy, T.T., Fällman, A.M., and Comans, R.N.J. (2005). Simultaneous application of dissolution/precipitation and surface complexation/surface precipitation modeling to contaminant leaching. *Environ. Sci. Technol.* 39, 5736.

Areco, M.M., Saleh-Medina, L., Trinelli, M.A., Marco-Brown, J.L., and dos Santos Afonso, M. (2013). Adsorption of Cu(II), Zn(II), Cd(II) and Pb(II) by dead *Avena fatua* biomass and the effect of these metals on their growth. *Colloid. Surface B* 110, 305.

Babaee, Y., Mulligan, C.N., and Rahaman, M.S. (2018). Removal of arsenic (III) and arsenic (V) from aqueous solutions through adsorption by Fe/Cu nanoparticles. *J. Chem. Technol. Biotechnol.* 93, 63.

Bee, S.-L., Abdullah, M.A.A., Bee, S.-T., Sin, L.T., and Rahmat, A.R. (2018). Polymer nanocomposites based on silylated-montmorillonite: A review. *Prog. Polym. Sci.* 85, 57.

Bhattacharyya, K.G., and Gupta, S.S. (2008). Adsorption of a few heavy metals on natural and modified kaolinite and montmorillonite: A review. *Adv. Colloid Interfac.* 140, 114.

Bhowmick, S., Chakraborty, S., Mondal, P., Van Renterghem, W., Van den Berghe, S., Roman-Ross, G., Chatterjee, D., and Iglesias, M. (2014). Montmorillonite-supported nanoscale zero-valent iron for removal of arsenic from aqueous solution: Kinetics and mechanism. *Chem. Eng. J.* 243, 14.

Brunauer, S., Emmett, P.H., and Teller, E. (1938). Adsorption of gases in multimolecular layers. *J. Am. Chem. Soc.* 60, 309.

Bundschuh, J., Litter, M., Ciminelli, V.S.T., Morgada, M.E., Cornejo, L., Hoyos, S.G., Hoinkis, J., Alarcón-Herrera, M.T., Armienta, M.A., and Bhattacharya, P. (2010). Emerging mitigation needs and sustainable options for solving the arsenic problems of rural and isolated urban areas in Latin America—A critical analysis. *Water Res.* 44, 5828.

Bundschuh, J., Litter, M.I., Parvez, F., Román-Ross, G., Nicolli, H.B., Jean, J.S., Liu, C.W., López, D., Armienta, M.A., Guilherme, L.R.G., Cuevas, A.G., Cornejo, L., Cumbal, L., and Toujaguez, R. (2012). One century of arsenic exposure in Latin America: A review of history and occurrence from 14 countries. *Sci. Total Environ.* 429, 2.

Chintala, R., Mollinedo, J., Schumacher, T.E., Papiernik, S.K., Malo, D.D., Clay, D.E., Kumar, S., and Gulbrandson, D.W. (2013). Nitrate sorption and desorption in biochars from fast pyrolysis. *Microporous Mesoporous Mater.* 179, 250.

Chowdhury, R. (2017). Using adsorption and sulphide precipitation as the principal removal mechanisms of arsenic from a constructed wetland—a critical review. *Chem. Ecol.* 33, 560.

Chowdhury, R., Apul, D., and Dwyer, D. (2008). Preliminary studies for designing a wetland for arsenic treatment. In L.F. König and J.L. Weiss, Eds., *Groundwater: Modeling Management*. Hauppage, NY: Nova Science Publishers, Inc., p. 155.

Corroto, C., Iriel, A., Cirelli, A.F., and Carrera, A.L.P. (2019). Constructed wetlands as an alternative for arsenic removal from reverse osmosis effluent. *Sci. Total Environ.* 691, 1242.

Di Rienzo, J.A., Casanoves, F., Balzarini, M.G., Gonzalez, L., Tablada, M., and Robledo, C.W. (2011). InfoStat. Universidad Nacional de Córdoba. Available at: www.infostat.com.ar (accessed April 2018).

Doğan, M., Abak, H., and Alkan, M. (2009). Adsorption of methylene blue onto hazelnut shell: Kinetics, mechanism and activation parameters. *J. Hazard. Mater.* 164, 172.

dos Santos Afonso, M., and Stumm, W. (1992). Reductive dissolution of iron(III) (hydr)oxides by hydrogen sulfide. *Langmuir* 8, 1671.

Essington, M.E. (2004). *Soil and Water Chemistry, an Integrative Approach.* Boca Raton, FL: CRC Press.

Flores, F.M., Torres Sánchez, R.M., and dos Santos Afonso, M. (2018). Some aspects of the adsorption of glyphosate and its degradation products on montmorillonite. *Environ. Sci. Pollut. Res. Int.* 25, 18138.

Gil, A., Assis, F.C.C., Albeniz, S., and Korili, S.A. (2011). Removal of dyes from wastewaters by adsorption on pillared clays. *Chem. Eng. J.* 168, 1032.

Grygar, T., Hradil, D., Bezdička, P., Doušová, B., Čapek, L., and Schneeweiss, O. (2007). Fe(III)-modified montmorillonite and bentonite: Synthesis, chemical and UV-Vis spectral characterization, arsenic sorption, and catalysis of oxidative dehydrogenation of propane. *Clay Clay Miner.* 55, 165.

Guo, J.Z., Li, B., Liu, L., and Lv, K. (2014). Removal of methylene blue from aqueous solutions by chemically modified bamboo. *Chemosphere* 111, 225.

Haerifar, M., and Azizian, S. (2013). Mixed surface reaction and diffusion-controlled kinetic model for adsorption at the solid/solution interface. *J. Phys. Chem.* 117, 8310.

Hayes, K.F., Papelis, C., and Leckie, J.O. (1988). Modeling ionic strength effects on anion adsorption at hydrous oxide/solution interfaces. *J. Colloid Interf. Sci.* 125, 717.

He, L.M., Zelazny, L.W., Baligar, V.C., Ritchey, K.D., and Martens, D.C. (1997). Ionic strength effects on sulfate and phosphate adsorption on γ-alumina and kaolinite: Triple-layer model. *Soil Sci. Soc. Am. J.* 61, 784.

Higuchi, T., and Connors, K. (1965). Phase solubility techniques. In C.N. Reilley, Ed., *Advances in Analytical Chemistry Instrumentation*. New York, NY: Interscience, p. 117.

Iriel, A., Dundas, G., Fernández Cirelli, A., and Lagorio, M.G. (2015a). Effect of arsenic on reflectance spectra and chlorophyll fluorescence of aquatic plants. *Chemosphere* 119, 697.

Iriel, A., Lagorio, M.G., and Fernández Cirelli, A. (2015b). Biosorption of arsenic from groundwater using Vallisneria gigantea plants. Kinetics, equilibrium and photophysical considerations. *Chemosphere* 138, 383.

Kazi, T.G., Arain, M.B., Baig, J.A., Jamali, M.K., Afridi, H.I., Jalbani, N., Sarfraz, R.A., Shah, A.Q., and Niaz, A. (2009). The correlation of arsenic levels in drinking water with the biological samples of skin disorders. *Sci. Total Environ.* 407, 1019.

Khoury, G.A., Gehris, T.C., Tribe, L., Torres Sánchez, R.M., and dos Santos Afonso, M. (2010). Glyphosate adsorption on montmorillonite: An experimental and theoretical study of surface complexes. *Appl. Clay Sci.* 50, 167.

Kumar, A., Gurian, P.L., Bucciarelli-Tieger, R.H., and Mitchell-Blackwood, J. (2008). Iron oxide—Coated fibrous sorbents for arsenic removal. *J. Am. Water Works Assoc.* 100, 151.

Lenoble, V., Bouras, O., Deluchat, V., Serpaud, B., and Bollinger, J.C. (2002). Arsenic adsorption onto pillared clays and iron oxides. *J. Colloid Interf. Sci.* 255, 52.

Li, Y., Liu, J.R., Jia, S.Y., Guo, J.W., Zhuo, J., and Na, P. (2012). TiO_2 pillared montmorillonite as a photoactive adsorbent of arsenic under UV irradiation. *Chem. Eng. J.* 191, 66.

Litter, M.I., Alarcón-Herrera, M.T., Arenas, M.J., Armienta, M.A., Avilés, M., Cáceres, R.E., Cipriani, H.N., Cornejo, L., Dias, L.E., Cirelli, A.F., Farfán, E.M., Garrido, S., Lorenzo, L., Morgada, M.E., Olmos-Márquez, M.A., and Pérez-Carrera, A. (2012). Small-scale and household methods to remove arsenic from water for drinking purposes in Latin America. *Sci. Total Environ.* 429, 107.

Litter, M.I., Ingallinella, A.M., Olmos, V., Savio, M., Difeo, G., Botto, L., Farfán Torres, E.M., Taylor, S., Frangie, S., Herkovits, J., Schalamuk, I., González, M.J., Berardozzi, E., García Einschlag, F.S., Bhattacharya, P., and Ahmad, A. (2019). Arsenic in Argentina: Occurrence, human health, legislation and determination. *Sci. Total Environ.* 676, 756.

Liu, G.J., Zhang, X.R., McWilliams, L., Talley, J.W., and Neal, C.R. (2008). Influence of ionic strength, electrolyte type, and NOM on As(V) adsorption onto TiO_2. *J. Environ. Sci. Health A* 43, 430.

Luengo, C., Puccia, V., and Avena, M. (2011). Arsenate adsorption and desorption kinetics on a Fe(III)-modified montmorillonite. *J. Hazard. Mater.* 186, 1713.

Marco-Brown, J.L., Areco, M.M., Torres Sánchez, R.M., and dos Santos Afonso, M. (2014). Adsorption of picloram herbicide on montmorillonite: Kinetic and equilibrium studies. *Colloid. Surface A* 449, 121.

Marco-Brown, J.L., Barbosa-Lema, C.M., Torres Sánchez, R.M., Mercader, R.C., and dos Santos Afonso, M. (2012). Adsorption of picloram herbicide on iron oxide pillared montmorillonite. *Appl. Clay Sci.* 58, 25.

Marco-Brown, J.L., Blesa, M.A., and Soler-Illia, G.J.A.A. (2017a). Preparation of mesoporous titania xerogels under controlled synthesis conditions. Effects of processing in the textural, adsorption and photocatalytic properties. *Colloid. Surface A* 530, 93.

Marco-Brown, J.L., Gaigneaux, E.M., Torres Sánchez, R.M., and dos Santos Afonso, M. (2019). Adsorption of picloram on clays nontronite, illite and kaolinite: Equilibrium and herbicide-clays surface complexes. *J. Environ. Sci. Health A* 54, 1.

Marco-Brown, J.L., Guz, L., Olivelli, M.S., Schampera, B., Torres Sánchez, R.M., Curutchet, G., and Candal, R. (2018). New insights on crystal violet dye adsorption on montmorillonite: Kinetics and surface complexes studies. *Chem. Eng. J.* 333, 495.

Marco-Brown, J.L., Trinelli, M.A., Gaigneaux, E.M., Torres Sánchez, R.M., and Dos Santos Afonso, M. (2015). New insights on the structure of the picloram-montmorillonite surface complexes. *J. Colloid Interf. Sci.* 444, 115.

Marco-Brown, J.L., Undabeytia, T., Torres Sánchez, R.M., and dos Santos Afonso, M. (2017b). Slow-release formulations of the herbicide picloram by using Fe–Al pillared montmorillonite. *Environ. Sci. Pollut. Res. Int.* 24, 10410.

Mohan, D., and Pittman, C.U., Jr. (2007). Arsenic removal from water/wastewater using adsorbents—A critical review. *J. Hazard. Mater.* 142, 1.

Murcott, S. (2012). *Arsenic Contamination in the World: An International Sourcebook.* London: IWA Publishing.

Partey, F., Norman, D.I., Ndur, S., and Nartey, R. (2009). Mechanism of arsenic sorption onto laterite iron concretions. *Colloid. Surface A* 337, 164.

Peng, X., Hu, F., Huang, J., Wang, Y., Dai, H., and Liu, Z. (2016). Preparation of a graphitic ordered mesoporous carbon and its application in sorption of ciprofloxacin: Kinetics, isotherm, adsorption mechanisms studies. *Microporous Mesoporous Mater.* 228, 196.

Reeve, N.G., and Sumner, M.E. (1971). Cation exchange capacity and exchangeable aluminum in natal oxisols. *Soil Sci. Soc. Am. Proc.* 35, 38.

Ren, X., Zhang, Z., Luo, H., Hu, B., Dang, Z., Yang, C., and Li, L. (2014). Adsorption of arsenic on modified montmorillonite. *Appl. Clay Sci.* 97–98, 17.

Rietveld, H. (1969). A profile refinement method for nuclear and magnetic structures. *J. Appl. Crystallogr.* 2, 65.

Sherlala, A.I.A., Raman, A.A.A., Bello, M.M., and Buthiyappan, A. (2019). Adsorption of arsenic using chitosan magnetic graphene oxide nanocomposite. *J. Environ. Manage.* 246, 547.

Siguín, D., Ferreira, S., Froufe, L., and García, F. (1994). Smectites: The relationship between their properties and isomorphic substitution. *J. Mater. Sci.* 29, 4379.

Sinha, D., Dey, S., Bhattacharya, R.K., and Roy, M. (2007). In vitro mitigation of arsenic toxicity by tea polyphenols in human lymphocytes. *J. Environ. Pathol. Toxicol. Oncol.* 26, 207.

Smedley, P.L., and Kinniburgh, D.G. (2002). A review of the source, behaviour and distribution of arsenic in natural waters. *Appl. Geochem.* 17, 517.

Smedley, P.L., Kinniburgh, D.G., Macdonald, D.M.J., Nicolli, H.B., Barros, A.J., Tullio, J.O., Pearce, J.M., and Alonso, M.S. (2005). Arsenic associations in sediments from the loess aquifer of La Pampa, Argentina. *Appl. Geochem.* 20, 989.

Stumm, W. (1992). *Chemistry of the Solid Water Interface. Processes at the Mineral-Water and Particle-Water Interface in Natural Systems*, 1st ed. New York: Wiley & Sons.

Sun, Q., and Yang, L. (2003). The adsorption of basic dyes from aqueous solution on modified peat–resin particle. *Water Res.* 37, 1535.

Timofeeva, M.N., Khankhasaeva, S.T., Chesalov, Y.A., Tsybulya, S.V., Panchenko, V.N., and Dashinamzhilova, E.T. (2009). Synthesis of Fe,Al-pillared clays starting from the Al,Fe-polymeric precursor: Effect of synthesis parameters on textural and catalytic properties. *Appl. Catal. B Environ.* 88, 127.

Tombácz, E., Csanaky, C., and Illés, E. (2001). Polydisperse fractal aggregate formation in clay mineral and iron oxide suspensions, pH and ionic strength dependence. *Colloid. Polym. Sci.* 279, 484.

Tschapek, M., Sanchez, R.M.T., and Wasowski, C. (1989). Handy methods for determining the isoelectric point of soils. *Z. Pflanz. Bodenkunde.* 152, 73.

Wang, Y., Zeng, X., Lu, Y., Bai, L., Su, S., and Wu, C. (2017). Dynamic arsenic aging processes and their mechanisms in nine types of Chinese soils. *Chemosphere* 187, 404.

Wang, Z., Hu, W., Kang, Z., He, X., Cai, Z., and Deng, B. (2019). Arsenate adsorption on iron-impregnated ordered mesoporous carbon: Fast kinetics and mass transfer evaluation. *Chem. Eng. J.* 357, 463.

Xu, F., Chen, H., Dai, Y., Wu, S., and Tang, X. (2019). Arsenic adsorption and removal by a new starch stabilized ferromanganese binary oxide in water. *J. Environ. Manage.* 245, 160.

Xu, R., Jiang, J., and Cheng, C. (2010). Effect of ionic strength on specific adsorption of ions by variable charge soils: experimental testification on the adsorption model of Bowden et al. In J. Xu and P.M. Huang, P.M., Eds., *Molecular Environmental Soil Science at the Interfaces in the Earth's Critical Zone*. Berlin, Heidelberg: Springer Berlin Heidelberg, p. 78.

Zhu, R., Chen, Q., Zhou, Q., Xi, Y., Zhu, J., and He, H. (2016). Adsorbents based on montmorillonite for contaminant removal from water: A review. *Appl. Clay Sci.* 123, 239.